

1
2
3
4
5
6 Contemporary Climate Change of the African Monsoon Systems
7
8
9

10 Kerry H. Cook and Edward K. Vizy
11
12 Department of Geological Sciences
13 The University of Texas at Austin
14
15

16
17
18
19
20
21
22
23
24
25
26
27
28
29
30 Citation:
31 Cook, KH, Vizy, EK, 2019: Contemporary Climate Change of the African Monsoon
32 SystemsCurrent Climate Change Reports, <http://link.springer.com/article/10.1007/s40641-019-00130-1>
33
34
35

36 **Purpose of Review**

37 Our current understanding of current climate change in the West African, East African, and Congo
38 Basin monsoon systems is reviewed. The detection of observed trends, the analysis of the physical
39 processes of change, and model projections are discussed.

40

41 **Recent Findings**

42 An increase in Sahel precipitation has been associated with a summer intensification and
43 northward shift of the West African monsoon system as a response to amplified warming over the
44 Sahara. Declines in the boreal spring rains over East Africa, and in spring and summer rains in the
45 Congo Basin, are also reported in the literature, but with less corroboration through physical
46 analysis and model projections. Confident analysis and accurate simulation are hampered by a
47 relative scarcity of observations in these regions.

48

49 **Summary**

50 The West African monsoon system is trending to bring more precipitation to the Sahel in summer,
51 and some is delivered through increasingly intense rainfall events. It is not yet clear whether recent
52 trends observed in the East African and Congo Basin monsoon systems can be expected to persist
53 as the global climate continues to warm. We cannot expect these monsoon systems to change
54 linearly through the 21st century because, as the ocean basins warm at different rates and with
55 different distributions, different forcing factors may become dominant.

56

57 **Keywords** climate change, monsoons, tropical rainfall, Sahel rainfall, East African precipitation,
58 Congo Basin, climate prediction

59 **I. Introduction**
60

61 Three regions of Africa are generally described as having monsoon climates, although the
62 historic definition of a seasonal reversal of the low-level wind direction may not apply everywhere.
63 Here we review recent research on climate change in the West African, East African, and Congo
64 Basin monsoon systems. While these regions are termed “monsoon systems”, they are not all
65 characterized by one summer rainy season. Rather, as mapped by Hermann and Mohr (2011),
66 some regions have complicated seasonality with multiple wet seasons that may or may not be
67 distinct from each other.

68 It is easy to motivate the study of climate change in these regions because the populations
69 are among the most vulnerable to climate change, including both in terms of economic loss and
70 mortality. Throughout the continent there is a high dependence on rain-fed agriculture, and many
71 regions have relatively low adaptive capabilities (Busby et al. 2014). The sheer size of Africa also
72 motivates its study - the surface area of the African continent exceeds the sum of the United States,
73 India, China, Japan, and most of Europe, yet the attention paid to the study of African climates is
74 far from proportional. African climate also influences regional and global climate. African wave
75 disturbances influence Atlantic hurricane development (e.g., Dieng et al. 2017) and the Sahara
76 Desert is estimated to emit 70% of the global total of mineral dust aerosols each year (Huneeus et
77 al. 2011) modifying global climate and weather (e.g., Pan et al. 2018), ocean and terrestrial
78 fertilization (e.g., Korte et al. 2017), and carbon sequestration in the deep ocean (Pabortsava et al.
79 2017).

80 Each of the three African monsoon climates is discussed below. We review background
81 on each that reflects our current knowledge, and follow this with a discussion of recent work aimed
82 at understanding the potential for – and reality of - climate change in African monsoon systems.

83

84 **II. The West African Monsoon System**

85

86 The West African summer monsoon season begins in late April or early May with the onset
87 of spring rains along the Guinean coast near 4°N. The Hovmöller diagram of the 1998-2017
88 TRMM Multisatellite Precipitation Analysis (TMPA; Huffman et al. 2007) daily precipitation
89 climatology averaged over West Africa between 12°W and 6°E (Fig. 1) shows that precipitation
90 intensifies through May until early June, and remains over the Guinean coast even as the marine
91 Atlantic ITCZ to the west moves farther north (Cook 2015), until late June or early July. At that
92 time, the rainfall maximum transitions into the southern Sahel, near 12°N, often over the course
93 of a few days.

94 This abrupt shift in the latitude of the rainfall maximum from the Guinean coast into the
95 Sahel is known as the West African monsoon jump (Sultan and Janicot 2000, 2003; Hagos and
96 Cook 2007; Peyrille et al. 2016). As seen in Fig. 1b, which shows the climatological time series
97 of rainfall over the Guinean coast and over the Sahel, the abruptness of the shift in the precipitation
98 maximum is associated with a rapid end of the springtime Guinean coast rainy season – Sahel
99 rainfall builds smoothly from May to a maximum in mid-August. The abrupt end of the spring
100 rains over the Guinean coast is associated with the seasonal movement of the African easterly jet
101 (AEJ), a mid-tropospheric jet that is controlled primarily by surface temperature gradients (Cook
102 1999; Thorncroft and Blackburn 1999; Wu et al. 2009). The strong negative meridional zonal
103 wind gradient over the coast that is associated with the AEJ preserves an inertially-stable
104 environment until the end of June. When the AEJ moves farther north, these gradients weaken
105 and reverse, satisfying the threshold condition for inertial instability. In the presence of this
106 instability, low-level convergence cannot be maintained, even over a surface temperature
107 maximum, and a rapid demise in the Guinean coast rainy season follows (Cook 2015). The

108 southward progression of the West African monsoon system is smooth because the inertial
109 instability mechanism does not apply for the equatorward movement of the AEJ. An early end of
110 the Sahel rainy season is associated with a strong North Atlantic subtropical anticyclone (NASH)
111 that extends eastward over the Mediterranean and Sahara (Zhang and Cook 2014). The opposite
112 occurs for a late rainfall demise. This is relevant for the 21st century as future projections from the
113 fifth phase of the Coupled Model Intercomparison Project (CMIP5; Taylor et al. 2012) indicate a
114 later demise in summer monsoon Sahel rainfall (Seth et al. 2013; Monerie et al. 2016).

115 The spring rainy season along the Guinean coast is supported primarily by the meridional
116 convergence of moisture-laden winds from the Gulf of Guinea (Fig. 1c; Sultan and Janicot 2003;
117 Nguyen et al. 2011; Thorncroft et al. 2011; Cook 2015; Schlueter et al. 2019), similar to the
118 hydrodynamics of the marine ITCZ. The Sahel rainy season is supported by moisture from the
119 Gulf and also from the eastern Atlantic by the low-level West African westerly jet (WAWJ). This
120 jet is distinguished from the meridional monsoon flow across the Guinean coast by its structure,
121 physical processes, variations, and connections with precipitation variability (Pu and Cook 2010,
122 2012; Liu et al. 2019).

123 On seasonal and sub-seasonal time scales, the Sahara thermal low, or West African heat
124 low, also has an important role in determining summer rainfall distributions over the Sahel (e.g.,
125 Lavaysse et al. 2009). During the boreal summer when heating is strongest over the Sahara, the
126 thermal low intensifies, enhancing the low-level transport of moisture over the West African Sahel
127 and southern Sahara needed to fuel convection (e.g., Parker et al. 2005; Lavaysse et al. 2009, 2010,
128 2016; Liu et al. 2019).

129 African easterly wave disturbances organize convection over large portions of West Africa.
130 Earlier investigations of these waves suggested that dynamical (shear) instability of the mid-level

131 African easterly jet (Burpee 1972; Cook 1999) generates them (Rennick 1976; Simmons 1977;
132 Thorncroft and Hoskins 1994; Thorncroft 1995). More recently, however, the strong concentration
133 of diabatic heating across the Sahel has been identified as the fundamental cause of the waves
134 (Hsieh and Cook 2005, 2007, 2008; Hall et al. 2006; Kiladis et al. 2006; Thorncroft et al. 2008).
135 The meridionally-narrow band of diabatic heating across the Sahel creates an environment (i.e.,
136 reversed potential vorticity gradients and Charney-Stern instability) that supports wave growth and
137 maintenance. Initial disturbances originate over the central Sahel and East Africa, including over
138 the Darfur Mountains and Ethiopian Highlands (Berry and Thorncroft 2005; Laing et al. 2008).
139 Vertical and meridional wind shears associated with the African easterly jet contribute to the scale
140 and structure of the waves. African easterly waves contribute to the organization of convection on
141 synoptic time scales (Mekonnen et al. 2006; Maranan et al. 2017; Vizy and Cook 2018a, b;
142 Schlueter et al. 2019), and help determine the diurnal cycle of rainfall (Zhang et al. 2016a).

143 Several papers document observed increases in rainfall amounts and intensity over the
144 West African monsoon region in recent decades, reversing a multi-decadal drying trend from the
145 late 1950s until the late 1980s. For example, shading in Figure 2a displays trends over the 1981-
146 2018 period from Climate Hazards group InfraRed Precipitation with Stations dataset (CHIRPS;
147 Funk et al. 2015b) for the height of the Sahel rainy season, the July-August-September mean, and
148 indicates positive precipitation trends across the Sahel. Studies by Sanogo et al. (2015), Barry et
149 al. (2018), Bicher and Diedhiou (2018), and Nicholson et al. (2018a) report overall positive trends
150 in large-scale precipitation and heavy rainfall days, but the trends are not necessarily monotonic
151 and exhibit some regionality. Panthou et al. (2018) also detect an intensification of rainfall in
152 daily ground-based observations in the Sahel, and they point out that the ongoing recovery of
153 rainfall amounts does not necessarily mean a return to the steadier pre-1950's rainfall regime.

154 The observed increases in Sahel rainfall amounts and intensity have been associated with
155 greenhouse-gas forcing in observational (Cook and Vizy 2015; Vizy and Cook 2017; Taylor et al.
156 2017) and model-based (Vizy et al. 2013; Dong and Sutton 2015; Han et al. 2019) analyses.
157 Warming over the Sahara Desert has been proceeding at an amplified pace – approximately triple
158 the rate of the tropical average, similar to the amplified warming of the Arctic (Cook and Vizy
159 2015). An examination of the surface heat budget indicates that the cause of the amplified
160 warming is primarily the dryness of the surface over the huge expanse of desert, although increases
161 in atmospheric water vapor content outside of the boundary layer play a role seasonally (Vizy and
162 Cook 2017). The resulting increase in the warm-season’s positive meridional temperature gradient
163 across West Africa (Fig. 2a) is accelerating the AEJ and enhancing southwesterly flow and
164 moisture transport into the Sahel. Taylor et al. (2017) suggest that the increased wind shear in the
165 Sahel intensifies convection, and increases in atmospheric water vapor may also play a role.

166 Vizy et al. (2013) find that the Sahara Desert’s amplified warming and related changes in
167 the atmospheric hydrodynamics occur both in regional model and CMIP5 AOGCM projections
168 under greenhouse gas-induced climate change, as shown in Figs. 2b-d. The regional model and
169 some of the AOGCMs translate these changes into significant Sahel precipitation increases by the
170 mid-21st c., and all models examined produce these effects by the end of the 21st c.

171 In addition to this sensitivity to the recent amplified Saharan warming, the West African
172 monsoon system is known to be sensitive to other local and global forcing. For example, the
173 influence of regional and remote SST forcing has been long identified as a primary forcing factor
174 of drought in the Sahel as highlighted in the review paper by Rodríguez-Fonseca et al. (2015), and
175 Lin et al. (2018) and Giannini and Kaplan (2018) also suggest a potential role for external aerosol
176 forcing. West Africa, and the Sahel in particular, is known to experience both short-term

177 (interannual) and long-term (decadal) droughts. The most notable long-term drought occurred
178 during the 1970s – 1980s (Nicholson 2013; Nicholson et al. 2018a). Since this time rainfall over
179 the Sahel has recovered to some extent. Occasional local and regional droughts still occur, and
180 they have become shorter and more frequent (Bicher and Diedhiou 2018; Han et al. 2019).
181 Variations in Atlantic SSTs characterized by warming in the equatorial Gulf of Guinea and cooling
182 off the West African coast north of 10°N are associated with a rainfall dipole over West Africa
183 with drying over the Sahel and enhanced rainfall along the Guinean Coast (Ward 1998; Vizy and
184 Cook 2002; Polo et al. 2008). Mediterranean SST anomalies also influence West African rainfall
185 variability, with warm SSTs associated with enhanced Sahel rainfall as the West African monsoon
186 shifts further north and intensifies (Rowell 2003; Fontaine et al. 2010).

187 Pacific and Indian Ocean SST anomalies can also impact rainfall variations over the Sahel
188 and West Africa. In some studies, warm tropical Pacific SSTs are associated with subsidence and
189 reduced rainfall over the Sahel during the peak of the summer monsoon (Mohino et al. 2011).
190 Indian Ocean warming has also been tied to Sahel drought, especially in the 1980s (Biasutti 2008;
191 Bader and Latif 2011; Fontaine et al. 2011), but Sahel rainfall has recovered since the 1990s while
192 Indian Ocean SSTs continue to warm. The response may depend on such factors as the spatial
193 scale of the Indian Ocean SSTs and interactions with SST forcing from other ocean basins (Suárez-
194 Moreno et al. 2018) including the Atlantic (Hagos and Cook 2008; Dyer et al. 2017a; Kamae et al.
195 2017).

196 Effects of changes in land-surface conditions are also discussed in the literature as a
197 mechanism for climate change over West Africa. Land cover over West Africa is changing as
198 more land is cultivated to support a growing population (Taylor et al. 2002; Wang et al. 2016).
199 These changes modify surface roughness and albedo, and can impact surface water distributions

200 and aerosol loading, affecting energy, momentum, and moisture exchanges between the surface
201 and atmosphere. In the 1960's and 70's, concern over declining rainfall in the Sahel led to wide-
202 spread acceptance of the so-called "Charney mechanism", in which deforestation in the Sahel was
203 thought to increase surface albedo and atmospheric stability, thereby decreasing rainfall (Charney
204 1975). This idea has been proven incorrect – the sensitivity arises in large part from a strong
205 boundary constraint in the original simple model used - and replaced by an understanding of the
206 dominate role of SST forcing on decadal time scales. This is not to say that West African rainfall
207 is completely insensitive to land-surface conditions. However, large-scale surface albedo changes
208 associated with human activity in West Africa are small and soil moisture feedbacks provide a
209 stronger forcing mechanism (Koster et al. 2006; Patricola and Cook 2008). In a recent review,
210 Spracklen et al. (2018) note the complexity of the issue, with deforestation leading to precipitation
211 reduction over the devegetated areas.

212 The Sahara is the largest source of atmospheric mineral dust, and is thought to suppress
213 severe storm activity in the tropical Atlantic and Caribbean, the southern U.S., and Europe as well
214 as within the West African monsoon (e.g., Lau et al. 2009; Chen et al. 2010; Knippertz et al. 2015,
215 2017; Bretl et al. 2015; Bahino et al. 2018; Pan et al. 2018). In addition to the Saharan dust, rapid
216 socioeconomic development in southern West Africa is increasing atmospheric loadings of
217 atmospheric pollutants, including particulate aerosols volatile organic particles (VOCs), with the
218 potential to modify the monsoon system through direct radiative effects and cloud interactions
219 (Deetz et al. 2018, Keita et al. 2018). However, even with high resolution and the inclusion of
220 explicit convection, climate and forecast models perform poorly in simulating African dust lifting
221 (Chaboureau et al. 2016), for example, in association with cold-pool outflows (haboobs) from the

222 numerous warm-season mesoscale convective systems (MCSs) that deliver West African rainfall
223 (e.g., Roberts et al. 2018) and low-level jets (Allen and Washington 2014).

224 With so many potentially potent forcing factors in play over such a large area with
225 nonlinear dynamics, it is probable that changes within the West African monsoon system as the
226 global climate warms will be non-linear (e.g., Neupane and Cook 2013) and regional. To support
227 prediction, there is a pressing need to continue progress on understanding the basic hydrodynamics
228 of the West African monsoon and the factors that cause this complex system to vary. Modeling at
229 convective-permitting (CP) resolutions (< 4 km) offers promise. Unlike GCMs, CP models are
230 able to capture the diurnal cycle of rainfall over West Africa (Zhang et al. 2016b), which requires
231 that both locally-generated and propagating mesoscale complexes are simulated accurately (Vizy
232 and Cook 2180a, b).

233

234 **III. The East African Monsoon System**

235 East Africa is a large area that extends some 40 degrees of latitude, from the Horn of Africa
236 (Ethiopia, Eritrea, Djibouti, and Somalia), through the equatorial region (Kenya, Uganda, Rwanda,
237 Burundi and Tanzania), to Mozambique and Malawi in the south. It is home to many of the most
238 food-insecure nations in the world according to the Food and Agriculture Organization of the
239 United Nations (FAO 2015) due to a dependence on rain-fed agriculture, low adaptive capability,
240 and the potential for climate-driven conflict. At least a portion of this insecurity derives from a
241 vulnerability to climate variability and change (O'Loughlin et al. 2012; Busby et al. 2014).
242 Climate is often viewed as a “threat multiplier” that is superimposed on other stressors in the
243 region.

244 Seasonality of the East African monsoon system is highly regional and complex. East
245 African rainfall is often described as having two rainy seasons – the “long rains” in boreal spring

246 and the “short rains” in boreal fall - that are related to “two passes” of the intertropical convergence
247 zone (ITCZ), but this is an over-simplification (e.g., Nicolson 2018). As shown by the
248 characterization of observed East African rainy seasons by Hermann and Mohr (2011), while some
249 regions of East Africa, for example, south-central Ethiopia, southern Somalia, and most of Kenya,
250 experience two, unimodal wet seasons, each with single peak, the remainder of Ethiopia, all of
251 Tanzania, and much of Southern Hemisphere East Africa (e.g., Malawi and Mozambique)
252 experience a single wet season in summer, sometimes with a mid-season break in precipitation
253 which is classified as a “bimodal regime”. The lack of zonal uniformity in the seasonal
254 characteristics of the East African monsoon and the presence of abrupt changes in the location of
255 rainfall maxima (Riddle and Cook 2008) indicates that the region’s rainfall cannot simply be
256 understood as the smooth movement of an ITCZ.

257 Many factors have been shown to influence East African rainfall, depending on location
258 and season. These factors include the region’s complicated topography and proximity to the Indian
259 Ocean, and sensitivity to global-scale modes of variability such as ENSO (e.g., Dunning et al.
260 2016). However, an understanding of the seasonality and variability of the highly regional
261 precipitation regimes is far from complete. As shown in Figure 3, there are significant seasonal
262 variations in the large-scale circulation (and moisture transports), including a reversal in wind
263 direction in DJF compared with the rest of the year. During the transition seasons (Figs. 3b and
264 d), on-shore flow brings moisture from the Indian Ocean to Southern Hemisphere East Africa,
265 while flow through the orographic gap known as the Turkana Channel (5°N, 36°E) and southerly
266 low-level flow channeled along the coast in part by the topography support Northern Hemisphere
267 precipitation. Due to warm Indian Ocean SSTs, the associated onshore transport of high moist
268 static energy is sufficiently large to overcome the divergence of the overlying air and produce a

269 rainy season over equatorial East Africa (Yang et al. 2015). Some of the large-scale moisture
270 transport patterns at 850 hPa that characterize boreal spring persist into the summer (Fig. 3c), with
271 added features due to the development of the West African summer monsoon system and the
272 development of the zonal branch of the Somali jet across the Arabian Sea supporting the single
273 rainy season of northern Ethiopia. The northeasterly flow of the Asian winter monsoon dominates
274 the circulation in DJF (Fig. 3a).

275 Because of this regional and seasonal complexity, evaluating East African rainfall trends
276 is not straightforward. Figure 4 shows the 1981-2018 CHIRPS linear precipitation trends over
277 East Africa for three seasons. CHIRPS incorporates 0.05° resolution satellite imagery with in-situ
278 station data to create gridded rainfall time series over land for trend analysis. We choose to show
279 it here because high spatial resolution is advantageous over the complex East African topography,
280 and the time series is relatively long (1981-present).

281 During boreal spring (Fig. 4a), drying trends with significance at the 90% level are evident
282 over central Somalia and the Ethiopian Highlands, with increasing precipitation trends around
283 Lake Victoria, west of the Ethiopian Highlands over Sudan and South Sudan, and eastern
284 Tanzania. Regions with weaker positive and negative trends are scattered.

285 In boreal summer (Fig. 4b), trends are small and incoherent over most of equatorial East
286 Africa where there is little rainfall, but positive trends associated with the Sahel rainfall recovery
287 occur over northern Ethiopia and the Sudan. Positive rainfall trends near Lake Victoria persist
288 through the summer and into the boreal fall (Fig. 4c), when the wetting trends extend over the
289 southern Ethiopian Highlands and the Turkana channel region, consistent with the gauge-based
290 analysis by Schmocker et al. (2016) for Mount Kenya. Farther south, there is evidence of

291 significant drying trends over southern Tanzania, northern Mozambique, and isolated areas of
292 Madagascar.

293 Recent impactful droughts (including the regional-scale drought of 2011 and another
294 centered in Ethiopia in 2015) heighten the concern about potential climatological precipitation
295 declines over East Africa. A number of recent papers evaluate East African rainfall trends, usually
296 for approximately the 1980-2010 time period for the spring long rains, and report negative trends
297 averaged across large areas (e.g., Lyon and DeWitt 2012; Funk et al. 2015a; Maidment et al. 2015).
298 There is especially a tendency for drying in the first decade of the 21st c. reported in the above
299 studies, although the exact location varies in different studies. For example, Ongoma and Chen
300 (2017) find a reduction in long rains (MAM) over Tanzania and Lake Victoria area in the 2001-
301 2010 decade, while Funk et al. (2015a) report reductions in the long rains (MAMJ) over northern
302 Tanzania, northern Kenya, and southeastern Ethiopia. These findings contrast with the results
303 shown in Fig. 4a, in which the spring drying is restricted to Ethiopia and Somalia. Analyses of the
304 trends associates the changes in rainfall with Indian Ocean SSTs and Walker circulation dynamics,
305 either due to natural variability or greenhouse gas increases (Williams and Funk 2011; Liebmann
306 et al. 2014; Yang et al. 2014), and western Pacific SSTs and/or the Pacific Decadal Oscillation
307 (Omondi et al. 2013, Yang et al. 2014, Funk et al. 2015c)

308 A trend in extreme events, including dry periods and intense rainfall, may be starting to
309 emerge over East Africa in observational analyses, but a clear picture has not yet formed. While
310 Grebrechorkos et al. (2019) do not find significant trends in rainfall extremes from 1981-2016 in
311 Ethiopia, Kenya, and Tanzania, Gummandi et al. (2018) report positive trends in precipitation
312 intensity over southern Ethiopia during both the spring and fall rainy seasons during a similar

313 period (1980-2010). These trends are accompanied by an increase in consecutive dry days as
314 precipitating systems intensify but become less frequent.

315 Projections of climate change over East Africa are hampered by the poor representation of
316 the rainy seasons in coupled GCMs. In Figs. 5a and, the black lines show the satellite-observed
317 TRMM rainfall climatology over a region in equatorial East Africa (primarily Kenya), with the
318 long rains in March, April and May and the short rains in October and November depicted. The
319 blue lines are rainfall averaged over the same region and 1986-2005 in two coupled GCMs
320 representative of the CMIP5 archive. In both models, the long rains are extremely weak, and the
321 short rains are too strong (see also Otieno and Anya 2013; Yang et al. 2015b; Rowell et al. 2015).
322 These inaccuracies in the simulations are, in some large part, associated with the ocean component
323 of the coupled GCMs – atmosphere only versions of the models with SSTs prescribed from
324 observations – produce much better simulations (purple lines in Figs. 5a and b). As seen in Fig.
325 5c, the 30-km, atmosphere-only regional model ensemble simulations of the late 20th c. described
326 in Vizy et al. (2013), also produce credible simulations of the East African rainy seasons.

327 Hiron and Turner (2018) relate the simulations of too-wet short rains in coupled GCMs
328 to mean-state biases in coupled GCMs, with easterly wind biases amplifying upwelling in the
329 eastern Indian Ocean and boreal fall precipitation. Yang et al. (2015b) compare coupled and
330 atmosphere-only versions of the MRI GCM and relate an improved simulation by the atmosphere-
331 only model to improvements in the low-level MSE and convective instability, ultimately related
332 to having a better representation of western Indian Ocean SSTs. Rowell and Chadwick (2018)
333 associate uncertainty in projections of East African rainfall with uncertainties in the regional
334 responses to projected SST warming in coupled GCMs. Strong influence from Indian Ocean SSTs
335 on East African rainfall is a major cause of the coupled models' rainfall inaccuracy, including the

336 ability to produce prominent modes of Indian Ocean SST variability (Weller and Cai 2013, Du et
337 al. 2013) and connections to ENSO (Ha et al. 2017).

338 Ummenhofer et al. (2018) shed some light on whether the poor simulation of the long rains
339 in a coupled GCM indicates that the model will be unable to accurately estimate changes in rainfall
340 due to greenhouse gas forcing (via SST anomalies) by examining observed modes of variability
341 and their connection to Indo-Pacific SSTs in a 1300-year simulation. They find that both the long
342 rains and the short rains respond to ENSO-like SSTAs, in contrast to observations in which the
343 only sensitivity is during the short rains. On decadal time scales, East African rainfall anomalies
344 were found to be responsive to Indian Ocean and Indo-Pacific, and not eastern Pacific, SSTA
345 variations, but these sensitivities were not well represented in the model.

346 The design of future simulations in a regional model skirts this problem to some extent by
347 generating future SSTs by adding coupled GCM-generated anomalies to observed present day
348 SSTs. This methodology depends on the ability of GCMs to project SST anomalies, but not on
349 their ability to produce a correct current SST distribution. The approach was first developed and
350 tested in paleoclimate applications by Cook and Vizy (2006) and Patricola and Cook (2007).
351 Under the RCP8.5 greenhouse-gas emissions scenario, ensemble simulations of the last 2 decades
352 of the 21st c. at 90-km (Cook and Vizy 2012, 2013) and 30-km resolution (as in Vizy et al 2013)
353 indicate little change in the long rains along the equator, and a strengthening of the short rains (red
354 line in Fig. 5c). Elsewhere in East Africa, the simulations project a weakening of the long rains
355 over Ethiopia and Somalia (similar to Fig. 4a) in connection with a strengthening of the Saharan
356 and Arabian highs, which has been related to amplified surface warming in these desert regions
357 (Cook and Vizy 2015; Vizy and Cook 2017).

358 As for the West African monsoon, CP-modeling holds promise for improving our ability
359 to simulate the East African monsoon system. Along with the usual benefits of explicitly resolving
360 convective processes in the governing equations rather than through parameterization, an added
361 benefit for East Africa is the accurate portrayal of the region's complex and influential topography.
362 More broadly, Finney et al. (2019) evaluate the benefits of CP modeling for the water budget
363 across East Africa and show that there are widespread improvements in rainfall intensity and
364 diurnal cycle in comparison with a coarser-resolution version of a similar model.

365
366 **IV. Congo Basin**
367

368 The monsoon system of equatorial western and central Africa, which we refer to here as
369 the Congo Basin region for efficiency, supports a tropical forest that is second in size to the
370 Amazon rainforest and the Congo River watershed which is the second-largest river basin on the
371 planet. The Congo River Basin, which is roughly equivalent to the monsoon region, covers $3.4 \times$
372 10^6 km^2 (nearly half the surface area of the contiguous U.S.) in central and western equatorial
373 Africa, including the Republic of Congo, the Democratic Republic of Congo, and the Central
374 African Republic, as well as portions of Tanzania, Cameroon, Angola, and Zambia. The Congo
375 Basin deforestation rate is estimated at 0.17% per year for 2000-2005, with additional degradation
376 (Ernst et al. 2012). This is much smaller than the deforestation rates in the Amazon, Central
377 America, and Southeast Asia forests, but it is nearly double the rate for the 1990-2000 period in
378 the Congo Basin and may change significantly in the future (Dargie et al. 2018).

379 Figure 4 displays a satellite-based estimate of the seasonal excursion of precipitation
380 averaged from 10°E to 30°E . Within 5° of latitude from the equator, precipitation persists for 10
381 months or more of the year. A broad swath of strong ($> 5 \text{ mm/day}$) precipitation progresses
382 smoothly from 10°S to 10°N from January through early August. After August, maximum rainfall

383 rates increase significantly, and the southward migration of the rainfall maximum occurs over 4
384 months.

385 Through most of the year, with the exception of boreal fall (DJF), southeasterly flow onto
386 the African continent from the South Indian Ocean transports large amounts of moisture into the
387 Congo Basin (Fig. 3). In JJA (Figs. 3c and d), this southeasterly flow is part of the full Somali jet
388 that consists of a southerly, cross-equatorial component and a zonal branch extending across the
389 Arabian Sea to India. At the 850 hPa level shown in Fig. 3, which clears much of the topography
390 as resolved in ERAI, a seasonal reversal of the meridional flow over the Congo Basin occurs.

391 An additional source of moisture for the Congo Basin is low-level westerlies from the
392 equatorial Atlantic, which are confined below 900 hPa (Pokam et al. 2012, Dezfuli and Nicholson
393 2013). Schwendike et al. (2014) and Pokam et al. (2014) discuss the existence of an over-turning
394 circulation, with a rising branch over the Congo Basin associated with descent over the equatorial
395 eastern Atlantic. Cook and Vizy (2016) show that the strength of this Congo Basin Walker
396 circulation is not correlated with land surface temperatures on seasonal time scales, and it only
397 exists in June through October when the Atlantic cold tongue is in place. Even then, the diabatic
398 heating maximum over the Congo Basin is primarily supported by inflow from the Indian Ocean
399 (see Dyer et al. 2017b), and the Congo Basin Walker circulation is not a closed system.

400 Even more than the other monsoon regions of Africa, the study of the Congo Basin
401 monsoon system is hampered by a lack of ground-based measurements of meteorological
402 variables. The number of reporting stations has declined over recent decades, especially since the
403 1980s in association with economic declines (Washington et al. 2013; Nicholson et al. 2018b).
404 This decrease hampers the evaluation and calibration of satellite-based observations, and can
405 introduce spurious trends (Maidment et al. 2015).

406 Mahli and Wright (2004) first raised concerns about a possible decline in Congo Basin
407 rainfall in analyzing CRU rain gauge data. Zhou et al. (2014) also suggested that precipitation
408 declines accompanied forest browning in boreal spring (April-May-June; AMJ) over the 2000-
409 2012 period. Maidment et al. (2015) examine trends in eight precipitation datasets for 1983-2010
410 and find disagreement among them over Central Africa, suggesting that spurious negative trends
411 associated with declines in gauge density occur in some datasets. Nicholson et al. (2018b)
412 produced gridded monthly-mean datasets at 2.5° and 5° resolution from gauge data for 1921-2014,
413 and examined AMJ trends in 14 sub-regions of the Congo Basin. Positive trends that are
414 significant at the 90th percentile are found in the northern portion (5°N – 10°N) of their analysis
415 region for the April, May, and June average, with negative trends elsewhere (10°S – 5°N), half of
416 which are significant.

417 Table 1, adapted from Cook et al. (2019), provides an overview of annual mean and
418 seasonal precipitation trends averaged over the entire Congo Basin for two time periods from six
419 datasets that are either satellite derived or based on blending satellite and gauge data. For the
420 annual mean over 1979-2017, all four available datasets produce negative trends, but only one is
421 statistically significant. For the six datasets analyzed for 1998-2017, all but one are negative, with
422 a highly significant negative trend in CHIRPS. Taken together, these data suggest annual-mean
423 Congo Basin drying, but confidence is not especially high.

424 Seasonal rainfall trends are also shown in Table 1. In DJF, negative trends predominate
425 for 1998-2017, but only CMORPH indicates high confidence. In boreal spring, represented as
426 MAM, negative linear trends that emerge weakly over the 1979-2017 period are not representative
427 of the 1998-2017 period, when positive precipitation trends (if anything) occur. (The result is
428 similar when boreal spring is represented by AMJ; negative trends for these months are more

429 significant for the 1979-2017 period, but also disappear for 1998-2017.) Negative trends emerge
430 most strongly, especially for the JJA period, during boreal summer. Cook et al. (2019) associate
431 these trends, and the somewhat less certain DJF trends, with poleward shifts in the thermal lows
432 over Africa. Given the findings of Guan et al. (2015) that the annual rainfall in the Congo Basin
433 is barely sufficient for maintaining the tropical forest, these reductions in rainfall even during the
434 less-rainy seasons may be critical. This is especially true if the poleward shifts of the thermal lows
435 will be continuing due to increasing greenhouse gas concentrations (as part of the observed tropical
436 expansion) and/or the recovery of the ozone hole in the Southern Hemisphere, or if possible boreal
437 spring rainfall reductions are related to warming SSTs (Hua et al. 2016).

438 Additional changes in Congo Basin rainfall are emerging in observations, especially for
439 extreme events. The Congo Basin climate is characterized by exceptionally strong MCS activity.
440 Taylor et al. (2018) find significant increases in intense rainfall events associated with MCS
441 activity since 1999 in February, suggesting an earlier onset of the boreal spring rainy season in
442 association with increasing meridional surface temperature gradients across the continent.

443 Large discrepancies in precipitation climatologies over the Congo Basin occur in the
444 current generation of coupled GCMs, and even the ensemble mean of CMIP5 historic simulations
445 likely does not produce a best estimate (Creese and Washington 2016). Discrepancies between
446 observed and modeled SSTs, especially in the southern Indian Ocean and the equatorial Atlantic,
447 may be related to the models' poor simulation of Congo Basin rainfall distributions, exacerbated
448 by the scarcity of observations with which to compare. However, even regional simulations at 30
449 km resolution with observed SSTs significantly over-produce Congo Basin rainfall in spring and
450 fall. In these simulations, the frequency of rainfall events is well-simulated, but precipitation rates
451 on wet days is too high (Han et al. 2019).

452 Adopting a more physically-based approach that emphasizes the transport and convergence
453 of moisture into the Congo Basin, and downplays the models' ability to translate this moisture into
454 precipitation using parameterizations, may provide leverage for extracting information about
455 Congo Basin climate change from AOGCMs. Creese and Washington (2018) explain and adopt
456 this approach for the boreal fall rainy season. During most of the year, models tend to have either
457 wet or dry biases throughout the basin. In boreal fall, however, biases in rainfall distributions
458 between the eastern and western basins are uncorrelated and this suggests associations with
459 physical processes may dominate. For example, they find that models with wet biases in the
460 western Congo Basin have unrealistically-warm SSTs in the eastern tropical Atlantic; models with
461 this characteristic may be less credible for predicting climate change in the Congo Basin.

462 The Congo Basin monsoon system is the least well-understood of the three African
463 monsoon systems reviewed here. Discrepancies in precipitation climatologies over the Congo
464 Basin produced by coupled GCMs and observational deficiency combine to raise considerable
465 uncertainty about climate change trends and future projections for the region and call for more
466 extensive study of this critical region.

467

468 **V. Concluding Remarks**

469 The school-book characterization of a monsoon climate is a region with strong seasonal
470 rainfall variations that are associated with land/sea contrasts and a seasonal reversal of winds. This
471 concept has led to suggestions that monsoon systems will intensify with increasing atmospheric
472 greenhouse gas levels as the land warms more quickly than the ocean. However, this simple
473 construct neglects the complexity and individuality of the world's monsoon systems in general,
474 and the African monsoon systems in particular. This review of the potential for climate change

475 in the African monsoons has emphasized the need for careful and in-depth regional study that is
476 based in the physical analysis of these complicated systems.

477 There is strong corroboration from observations and modeling, combined with a physical
478 understanding of the processes, that amplified warming over the Sahara due to increasing
479 greenhouse gas levels is contributing to positive precipitation trends over the Sahel. Indian Ocean
480 warming is likely playing a supportive role as well. These increases represent an intensification
481 and northward shift of the West African monsoon system during boreal summer. However, this
482 does not mean that we can be sure that this positive trend will continue through the 21st century.
483 The sensitivity of the West African monsoon system, including its association with rainfall along
484 the Guinean Coast as well as over the Sahel, to SSTs is well known. For example, from analysis
485 on interannual time scales, we know that warming SSTs in the Gulf of Guinea in isolation are
486 associated with increased rainfall along the coast and reduced rainfall over the Sahel.
487 Consequently, as the ocean basins warm at different rates and with different distributions over the
488 21st century, other forcing factors may become dominant over the amplified-Sahara-warming
489 mechanism.

490 Over East Africa, several papers report a decline in the historical long rains, but results
491 depend on the exact analysis periods and averaging regions. The precipitation decreases are
492 especially strong in the first decade of the 21st c., but the presence of an ongoing trend has not been
493 established. This monsoon system is characterized by extremely strong regionality associated with
494 its complex topography and geographical location. Regional rainfall has strong coupling with the
495 Indian Ocean, which provides much of the moisture advected into East Africa, but the mechanisms
496 that control the convergence of that moisture and atmospheric stability are not well known.

497 The monsoon system that supplies moisture to the Congo Basin also exhibits strong
498 coupling with the Indian Ocean. Reports of boreal spring drying are not yet certain, but they are
499 of great concern since the region's tropical forests are thought to receive marginal rainfall amounts.
500 Poleward shifts of the African continental thermal lows in both hemispheres can lead to Congo
501 Basin drying since the equatorward flow to the east of the lows supports moisture convergence
502 over central and eastern equatorial Africa. Improved understanding of the region hinges on
503 improvements in both observations and modeling.

504 Perhaps more than other regions of the world, African monsoon systems are dependent on
505 SSTs in seasonally- and regionally-dependent ways. This dependence suggests that we may not
506 be able to fully understand climate change in these regions without fully-confident projections of
507 SST distributions, especially in the Atlantic and Indian Oceans. However, there are also local
508 processes to consider that are currently not well understood, including regional circulation
509 systems, connections among the African monsoon systems, and the role of complex topography,
510 not to mention the MCSs that deliver up to 80% of the rainfall and control impactful intense events
511 and the diurnal cycle of rainfall.

512 With so many potentially potent forcing factors in play over such a large area, it is probable
513 that changes within the African monsoon systems as the global climate warms will be non-linear
514 and highly regional. To support prediction, there is a pressing need to continue progress on
515 understanding the basic hydrodynamics of the African monsoon systems and the factors that cause
516 these complex systems to vary on different time scales.

517

518 **Acknowledgements:** Support from NSF Awards #1701520 and #1444505 is gratefully
519 acknowledged. The Texas Advanced Computing Center (TACC) at The University of Texas at

520 Austin provided database resources, and the Grid Analysis and Display System software (GrADS)
521 developed at COLA/IGES was used for generating the figures. We also thank Dr. Richard
522 Washington and an anonymous reviewer for their helpful comments which improved the paper.

523

524 On behalf of both authors, the corresponding author states that there is no conflict of interest.

525

526 **References**

527 Allen CJT, Washington R (2014) The low-level jet dust emission mechanism in the central Sahara:
528 Observations from Bordj-Badji Mokhtar during the June 2011 Fennec intensive
529 observation period. *J. Geophy. Res: Atmospheres* 119: 2990-3015. <https://doi:10.1002/2013JD020594>.

531 Bader J, Latif M (2011) The 1983 drought in the West Sahel: A case study. *Clim Dyn* 36: 463-
532 472. <https://doi.org/10.1007/s00382-009-0700-y>

533 Bahino J, Yoboué V, Galy-Lacaux C, Adon M, Akpo A, Keita S, Liousse C, Gardrat E, Chiron C,
534 Ossouhou M, Gnamien S, Djossou J (2018) A pilot study of gaseous pollutants'
535 measurement (NO₂, SO₂, NH₃, HNO₃ and O₃) in Abidjan, Côte d'Ivoire: Contribution to
536 an overview of gaseous pollution in African cities. *Atmos Chem Phys* 18: 5173–5198.
537 <https://doi.org/10.5194/acp-18-5173-2018>

538 Barry AA, Caesar J, Klein Tank AMG, Aguilar E, McSweeney C, and co-authors (2018) West
539 Africa climate extremes and climate change indices. *Int J Climatol* 38: e921-e938.
540 <https://doi.org/10.1002/joc.5420>

541 Berry GJ, Thorncroft C (2005) Case study of an intense African easterly wave. *Mon Wea. Rev*
542 133: 752-766. <https://doi.org/10.1175/MWR2884.1>

543 Biasutti M (2008) SST forcings and Sahel rainfall variability in simulations of the twentieth and
544 twenty-first centuries. *J Climate* 21: 3471-3486. <https://doi.org/10.1175/2007JCLI1896.1>

545 Bicher A, Diedhiou A (2018) West African Sahel has become wetter during the last 30 years, but
546 dry spells are shorter and more frequent. *Clim Res* 75: 155-162.
547 <https://doi.org/10.3354/cr01515>

548 Bretl S, Reutter P, Raible CC, Ferrachat S, Poberaj CS, Revell LE, Lohmann U (2015) The
549 influence of absorbed solar radiation by Saharan dust on hurricane genesis. *J Geophys Res
550 Atmos* 120: 1902–1917. <https://doi.org/10.1002/2014JD022441>

551 Burpee RW (1972) The origin and structure of easterly waves in the lower troposphere of North
552 Africa. *J Atmos Sci* 29: 77-90. [https://doi.org/10.1175/1520-0469\(1972\)029<0077:TOASOE>2.0.CO;2](https://doi.org/10.1175/1520-
553 0469(1972)029<0077:TOASOE>2.0.CO;2)

554 Busby JW, Cook KH, Vizy EK, Smith TG, Bekalo M (2014) Identifying hot spots of security
555 vulnerability associated with climate change in Africa. *Climatic Change* 124: 717-731.
556 <https://doi.org/10.1007/s10584-014-1142-z>

557 Chaboureau J-P, Flamant C, Kocha C, and co-authors (2016) Fennec dust forecast intercomparison
558 over the Sahara in June 2011. *Atmos Chem Phys* 16: 6977-6995.
559 <https://doi.org/10.5194/acp-6977-2016>

560 Charney JG (1975) Dynamics of deserts and drought in the Sahel. *Quart J Roy Meteor Soc* 101:
561 193–202. <https://doi.org/10.1002/qj.49710142802>

562 Chen S-H, Wang S-H, Waylonis M (2010) Modification of Saharan air layer and environmental
563 shear over the eastern Atlantic Ocean by dust-radiation effects. *J Geophys Res* 115:
564 D21202. <https://doi.org/10.1029/2010JD014158>

565 Cook KH (1999), Generation of the African easterly jet and its role in determining West African
566 precipitation, J Climate 12: 1165–1184. [https://doi.org/10.1175/1520-0442\(1999\)012<1165:GOTAEJ>2.0.CO;2](https://doi.org/10.1175/1520-0442(1999)012<1165:GOTAEJ>2.0.CO;2)

567

568 Cook KH (2015) Role of inertial instability in the West African Monsoon Jump. J Geophys Res -
569 Atmos 120: 3085-3102. <https://doi.org/10.1002/2014JD022579>

570 Cook KH, Liu Y, Vizy EK (2019) Congo Basin drying associated with poleward shifts of African
571 thermal lows. Under review Clim Dyn.

572 Cook KH, Vizy EK (2006) South American climate during the Last Glacial Maximum: Delayed
573 onset of the South American monsoon. J Geophys Res Atmos 111 (D2): 2110.
574 <https://doi.org/10.1029/2005JD005980>

575 Cook KH, Vizy EK (2012) Impact of climate change on mid-21st century growing seasons in
576 Africa. Clim Dyn 39: 2937-2955. <https://doi.org/10.1007/s00382-012-1324-1>

577 Cook KH, Vizy EK (2013) Projected changes in East African rainy seasons. J Climate 26: 5931-
578 5948. <https://doi.org/10.1175/JCLI-D-12-00455.1>

579 Cook KH, Vizy EK (2015) Detection and analysis of an amplified warming of the Sahara Desert.
580 J Clim 28: 6560-6580. <https://doi.org/10.1175/JCLI-D-14-00230.1>

581 Cook KH, Vizy EK (2016) The Congo basin Walker circulation: Dynamics and connections to
582 precipitation. Clim Dyn 47: 697-717. <https://doi.org/10.1007/s00382-015-2864-y>

583 Creese A, Washington R (2016) Using qflux to constrain modeled Congo Basin rainfall in the
584 CMIP5 ensemble. J Geophys Res 121: 13415-13442.
585 <https://doi.org/10.1002/2016JD025596>

586 Creese, A, Washington R (2018) A process-based assessment of CMIP5 rainfall in the Congo
587 Basin: The September-November rainy season. *J Climate* 31: 7417-7439.
588 <https://doi.org/10.1175/JCLI-D-17-0818.1>

589 Dargie GC, Lawson IT, Rayden TJ, Miles L, Mitchard ET, Page SE, Bocko YE, Ifo SA, Lewis SL
590 (2109). Congo Basin peatlands: threats and conservation priorities. *Mitigation and*
591 *Adaptation Strategies for Global Change*: 24 <https://doi.org/10.1007/s11027-017-9774-8>

592 Deetz K, Vogel H, Knippertz P, and co-authors (2018) Numerical simulations of aerosol radiative
593 effects and their impact on clouds and atmospheric dynamics over southern West Africa.
594 *Atmos Chem Phys* 18: 9767-9788. <https://doi.org/10.5194/acp-18-9767-2018>

595 Dezfuli AK, Nicholson SE (2013) The relationship of rainfall variability in western Equatorial
596 Africa to the tropical oceans and atmospheric circulation. Part II: The boreal autumn. *J*
597 *Climate* 26: 66-84. <https://doi.org/10.1175/JCLI-D-11-00686.1>

598 Dieng AL, Sall SM, Eymard L, Leduc-Leballeur M, Lazar A (2017) Trains of African easterly
599 waves and their relationship to tropical cyclone genesis in the eastern Atlantic. *Mon Wea*
600 *Rev* 145: 599-616. <https://doi.org/10.1175/MWR-D-15-0277.1>

601 Dong B, Sutton R (2015) Dominant role of greenhouse-gas forcing in the recovery of Sahel
602 rainfall. *Nature Clim Change* 5: 757-760. <https://doi.org/10.1038/NCLIMATE2664>

603 Du Y, Cai W, Wu Y (2013) A new type of the Indian Ocean dipole since the mid-1970s. *J Climate*
604 26: 959-972. <https://doi.org/10.1175/JCLI-D-12-00047.1>

605 Dunning, CM, Black ECL, and Allan RP (2016) The onset and cessation of seasonal rainfall over
606 Africa, *J. Geophys. Res. Atmos.* 121: 11,405-11,424, <https://doi.org/10.1002/2016JD025428>

607 Dyer ELE, Jones DBA, Li R, Sawaoka H, Mudryk L (2017a) Sahel precipitation and regional
608 teleconnections with the Indian Ocean. *J Geophy Res Atmos* 122: 5654-5676.
609 <https://doi.org/10.1002/2016JD026014>

610 Dyer ELE, Jones DB, Nusbaumer J, Li H, Collins O, Vettoretti G, Noone D (2017b) Congo
611 Basin precipitation: Assessing seasonality, regional interactions, and sources of moisture.
612 *J Geophys Res* 122: 6882-6898. <https://doi.org/10.1002/2016JD026240>

613 Ernst C, Mayaux P, Verhegghen A, Bodart C, Christophe M, Defourny P (2013) National forest
614 cover change in Congo Basin: deforestation, reforestation, degradation and regeneration
615 for the years 1990, 2000 and 2005. *Glob Change Biol* 19: 1173-1187.
616 <https://doi:10.1111/gcb.12092>

617 Finney DL, Marsham JH, Jackson LS, Kendon EJ, Rowell DP, Boorman PM, Keane RJ, Stratton
618 RA, Senior CA (2019) Implications of improved representation of convection for the East
619 Africa water budget using a convective-permitting model. *J. Climate* 32: 2109-2129.

620 Food and Agriculture Organization of the United Nations (FAO), 2015: The State of Food
621 Insecurity in the World 2015. <http://www.fao.org/hunger/en/>

622 Fontaine B, and co-authors (2010) Impacts of warm and cold situations in the Mediterranean basins
623 on the West African monsoon: Observed connection patterns (1979–2006) and climate
624 simulations. *Clim Dyn* 35: 95–114. <https://doi.org/10.1007/s00382-009-0599-3>

625 Fontaine B, Monerie P-A, Gaetani M, Roucou P (2011) Climate adjustments over the African-
626 Indian monsoon regions accompanying Mediterranean Sea thermal variability. *J Geophys
627 Res Atmos* 116: D23122. <https://doi.org/10.1029/2011JD016273>

628 Funk C, Hoell A, Husak G, Shukla S, Michaelsen J (2015a) The East African monsoon system:
629 seasonal climatologies and recent variations. Chapter for “The Monsoons and Climate

630 Change”, Leila M. V. Carvalho and Charles Jones (Eds.). <https://doi.org/10.1007/978-3->
631 319- 21650-8_1

632 Funk C, Peterson P, Landsfeld M, Pedreros D, Verdin J, Shukla S, Husak G, Rowland J, Harrison
633 L, Hoell A, Michaelsen J (2015b) The climate hazards infrared precipitation with stations
634 – a new environmental record for monitoring extremes. *Scientific Data* 2: 150066.
635 <https://doi.org/10.1038/sdata.2015.66>

636 Funk C, Shukla S, Hoell A, Livneh B (2015c) Assessing the contributions of east African and west
637 pacific warming to the 2014 boreal spring east African drought [in “Explaining Extremes
638 of 2014 from a Climate Perspective”]. *Bull. Amer. Meteor. Soc.* 96: S5–S9.

639 Giannini A, Kaplan A. (2018) The role of aerosols and greenhouse gases in Sahel drought and
640 recovery. *Climatic Change*. <https://doi.org/10.1007/s10584-018-2341-9>

641 Grebrechorkos S, Hulsmann S, Bernhofer C (2019) Changes in temperature and precipitation
642 extremes in Ethiopia, Kenya, and Tanzania. *Int J Climatol* 39: 18-30.
643 <https://doi.org/10.1002/joc.5777>

644 Guan K, Pan M, Haiban L, and co-authors (2015) Photosynthetic seasonality of global tropical
645 forests constrained by hydroclimate. *Nature Geoscience* 8: 284-289.
646 <https://doi.org/10.1038/NGEO2382>

647 Gummadi S, Rao KPC, Seid J, Legesse G, Kadiyala MDM, Takele R, Amede T, Whitbread A
648 (2018) Spatio-temporal variability and trends of precipitation and extreme rainfall events
649 in Ethiopia in 1980-2010. *Theoretical and Applied Climatology* 134: 1315-1328.
650 <https://doi.org/10.1007/s00704-17-2340-1>

651 Ha KJ, JE Chu, JY Lee, KS Yun (2017) Interbasin coupling between the tropical Indian and
652 Pacific Ocean on interannual timescale: Observation and CMIP5 reproduction. *Climate
653 Dynamics*, 48, 459-475. <https://doi.org/10.1007/s00382-016-3087-6>

654 Hagos SM, Cook KH (2007) Dynamics of the West African monsoon jump, *J Clim* 20: 5264–
655 5284. <https://doi.org/10.1175/2007JCLI1533.1>

656 Hagos S, Cook KH (2008) Ocean warming and late-twentieth-century Sahel drought and recovery.
657 *J Climate* 21: 3797–3814, <https://doi.org/10.1175/2008JCLI2055.1>

658 Hall NMJ, Kiladis GN, Thorncroft CD (2006) Three-dimensional structure and dynamics of
659 African easterly waves. Part II: Dynamical modes. *J Atmos Sci* 63: 2231–2245.
660 <https://doi.org/10.1175/JAS3742.1>

661 Han, F, Cook KH, Vizy EK, 2019: Changes in Intense Rainfall Events and Drought Across Africa
662 in the 21st Century. *Climate Dynamics* <https://doi.org/10.1007/s00382-019-04653-z>

663 Herrmann SM, Mohr KI (2011) A continental-scale classification of rainfall seasonality regimes
664 in Africa based on gridded precipitation and land surface temperature products. *J Appl
665 Meteorol Climatol* 50: 2504-2513. <https://doi.org/10.1175/JAMC-D-11-024.1>

666 Hirons L, Turner A (2018) The impact of Indian Ocean mean-state biases in climate models on
667 the representation of the East African short rains. *Journal of Climate*, 3: 6611-6631

668 Hsieh J-S, Cook KH (2005) Generation of African easterly wave disturbances: Relationship to the
669 African easterly jet. *Mon Wea Rev* 133: 1311-1327. <https://doi.org/10.1175/MWR2916.1>

670 Hsieh J-S, Cook KH (2007) A study of the energetics of African easterly waves using a regional
671 climate model. *J Atmos Sci* 64: 421-440. <https://doi.org/10.1175/JAS3851.1>

672 Hsieh J-S, Cook KH (2008) On the instability of the African easterly jet and the generation of
673 African waves: Reversals of the potential vorticity gradient. *J Atmos Sci* 65: 2130-2151.
674 <https://doi.org/10.1175/2007JAS2552.1>

675 Hua W, Zhou L, Chen H, Nicholson SE, Jiang Y, Raghavendra A (2016) Possible causes of the
676 Central Equatorial African long-term drought. *Environ Res Lett* 11: 124002.
677 <https://doi.org/10.1088/1748-9326/11/12/124002>

678 Huffman GJ, Adler RF, Bolvin DT, Gu G, Nelkin EJ, Bowman KP, Hong Y, Stocker EF, Wolff
679 DB (2007) The TRMM multisatellite precipitation analysis (TMPA): quasi-global,
680 multiyear, combined-sensor precipitation estimates at fine scales. *J Hydrometeorol* 8:38–
681 55. <https://doi.org/10.1175/JHM560.1>

682 Huneeus N, and co-authors (2011) Global dust model intercomparison in AeroCom phase I. *Atmos*
683 *Chem Phys* 11: 7781-7816. <https://doi.org/10.5194/acp-11-7781-2011>

684 Kamae Y, Li X, Xie S-P, Ueda H (2017) Atlantic effects on recent decadal trends in global
685 monsoon. *Clim Dyn* 43: 3443. <https://doi.org/10.1007/s00382-017-3522-3>

686 Keita S, Lioussse C, and co-authors (2018) Particle and VOC emission factor measurements for
687 anthropogenic sources in West Africa. *Atmos Chem Phys* 18: 7691-7708.
688 <https://doi.org/10.5194/acp-18-7691-2018>

689 Kiladis GN, Thorncroft CD, Hall NMJ (2006) Three-dimensional structure and dynamics of
690 African easterly waves. Part I: Observations. *J Atmos Sci* 63: 2212–2230.
691 <https://doi.org/10.1175/JAS3741.1>

692 Knippertz P, Coe H, Chiu JC, Evans MJ, Fink AH, Kalthoff N, Lioussse C, Mari C, Allan RP,
693 Brooks B, Danour S, Flamant C, Jegede OO, Fabienne L, Marsham JH (2015) The

694 DACCIWA Project. Bull Amer Meteorol Soc 96: 1451– 1460.

695 <https://doi.org/10.1175/BAMS-D-14-00108.1>

696 Knippertz P, Fink AH, Deroubaix A, Morris E, Tocquer F, Evans MJ, Flamant C, Gaetani M,

697 Lavaysse C, Mari C, Marsham JH, Meynadier R, Affo-Dogo A, Bahaga T, Brosse F, Deetz

698 K, Guebsi R, Latifou I, Maranan M, Rosenberg PD, Schlüter A (2017) A meteorological

699 and chemical overview of the DACCIWA field campaign in West Africa in June-July

700 2016. *Atmos Chem Phys* 17: 10893–10918, <https://doi.org/10.5194/acp-17-10893-2017>

701 Korte LF, Brummer G-JA, and co-authors (2017) Downward particle fluxes of biogenic matter

702 and Saharan dust across the equatorial North Atlantic. *Atmos Chem Phys* 17: 6023-6040.

703 <https://doi.org/10.5194/acp-17-6023-2017>

704 Koster RD, and co-authors (2006) GLACE: The Global Land–Atmosphere Coupling Experiment.

705 Part I: Overview. *J Hydrometeor* 7: 590–610. <https://doi.org/10.1175/JHM510.1>

706 Laing AG, Carbone R, Levizzani V, Tuttle J (2008) The propagation and diurnal cycles of deep

707 convection in northern tropical Africa. *Q J R Meteorol Soc* 134: 93-109.

708 <https://doi.org/10.1002/qj.194>

709 Lau KM, Kim KM, Sud YC, Walker GK (2009) A GCM study of the response of the atmospheric

710 water cycle of West Africa and the Atlantic to Saharan dust radiative forcing. *Ann Geophys*

711 27: 4023–4037. <https://doi.org/10.5194/angeo-27-4023-2009>

712 Lavaysse C, Flamant C, Evan A, Janicot S, Gaetani M (2016) Recent climatological trend of the

713 Saharan heat low and its impact on the West African climate. *Clim Dyn* 47: 3479-3498.

714 <https://doi.org/10.1007/s00382-015-2847-z>

715 Lavaysse C, Flamant C, Janicot S (2010) Regional-scale convection patterns during strong and
716 weak phases of the Saharan heat low. *Atmos Sci Lett* 11(4):255–264.
717 <https://doi.org/10.1002/asl.284>

718 Lavaysse C, Flamant C, Janicot S, Parker DJ, Lafore JP, Sultan B, Pelon J (2009) Seasonal
719 evolution of the West African heat low: a climatological perspective. *Clim Dyn* 33(2–
720 3):313–330. <https://doi.org/10.1007/s00382-009-0553-4>

721 Liebmann B, Hoerling MP, Funk C, Bladé I, Dole RM, Allured D, Quan X, Pegion P, Eischeid JK
722 (2014) Understanding recent Horn of Africa rainfall variability and change. *J Climate* 27:
723 8629–8645. <https://doi.org/10.1175/JCLI-D-13-00714.1>

724 Lin L, Wang ZL, Xu YY, Fu Q, Dong WJ (2018) Larger sensitivity of precipitation extremes to
725 aerosol than greenhouse gas forcing in CMIP5 models. *J Geophys Res – Atmos* 123: 8062–
726 8073. <https://doi.org/10.1029/2018JD028821>

727 Liu W, Cook KH, Vizy EK (2019) Role of the West African westerly jet in the seasonal and diurnal
728 cycles of precipitation over West Africa. Submitted *Clim Dyn*.

729 Lyon B, DeWitt DG (2012) A recent and abrupt decline in East African long rains. *Geophys Res*
730 *Lett* 39: L02702. <https://doi.org/10.1029/2011GL050337>

731 Maidment RI, Allan RP, Black E (2015) Recent observed and simulated changes in precipitation
732 over Africa. *Geophys Res Lett* 42: 8155–8164. <https://doi.org/10.1002/2015GL065765>

733 Malhi Y, Wright J (2004) Spatial patterns and recent trends in the climate of tropical rainforest
734 regions. *Phil Trans R Soc Lond B* 359: 311–329. <https://doi.org/10.1098/rstb.2003.1433>

735 Maranan M, Fink AH, Knippertz P (2017) Rainfall types over southern West Africa: Objective
736 identification, climatology and synoptic environment. *Q J Roy Meteorol Soc* 144: 1628–
737 1648. <https://doi.org/10.1002/qj.3345>

738 Mekonnen A, Thorncroft CD, Aiyyer A (2006) Analysis of convection and its association with
739 African easterly waves. *J Climate* 19: 5405–5421. <https://doi.org/10.1175/JCLI3920.1>

740 Mohino E, Mechoso CR, Gervois S, Ruti P, Chauvin F (2011c) Impacts of the tropical
741 Pacific/Indian Oceans on the seasonal cycle of the West African monsoon. *J Climate* 24:
742 3878-3891. <https://doi.org/10.1175/2011JCLI3988.1>

743 Monerie P-A, Biasutti M, Roucou P (2016) On the projected increase of Sahel rainfall during the
744 late rainy season. *Int J Climatol* 36: 4373-4383. <https://doi.org/10.1002/joc.4638>

745 Neupane N, Cook KH (2013) A nonlinear response of Sahel rainfall to Atlantic warming. *J Climate*
746 26: 7080-7096. <https://doi.org/10.1175/JCLI-D-12-00475.1>

747 Nguyen H, Thorncroft CD, Zhang C (2011) Guinean coastal rainfall of the West African monsoon.
748 *Q J R Meteorol Soc* 137: 1828-1840. <https://doi.org/10.1002/qj.867>

749 Nicholson SE (2013) The West African Sahel: A review of recent studies on the rainfall regime
750 and its interannual variability. *ISRN Meteorology* 2013: 453521.
751 <https://doi.org/10.1155/2013/453521>

752 Nicholson SE (2018) The ITCZ and the seasonal cycle over Equatorial Africa. *Bull Amer Meteorol
753 Soc* 99: 337-348. <https://doi.org/10.1175/BAMS-D-16-0287.1>

754 Nicholson SE, Fink AH, Funk C (2018a) Assessing recovery and change in West Africa's rainfall
755 regime from a 161-year record. *Int J Climatol* 38: 3770-3786.
756 <https://doi.org/10.1002/joc.5530>

757 Nicholson SE, Klotter D, Dezfuli AK, Zhou L (2018b) New rainfall datasets for the Congo basin
758 and surrounding regions. *J Hydrometeor* 19: 1379-1396. [https://doi.org/10.1175/JHM-D-18-0015.1](https://doi.org/10.1175/JHM-D-
759 18-0015.1)

760 O'Loughlin J, Witmer FDW, Linke AM, Laing A, Gettelman A, Dudhia J (2012) Climate
761 variability and conflict risk in East Africa, 1990-2009. *Proceedings Nat Acad Sci* 109:
762 18344-18349. <https://doi.org/10.1073/pnas.1205130109>

763 Omondi P, Ogallo LA, Anya R, Muthama JM, Ininda J, 2013: Linkages between global sea surface
764 temperatures and decadal rainfall variability over Eastern Africa region. *Int. J. Climatology*
765 33:2082-2104.

766 Ongoma V, Chen H (2017) Temporal and spatial variability of temperature and precipitation over
767 East Africa from 1951 to 2010. *Meteorol Atmos Phys* 129: 131-144.
768 <https://doi.org/10.1007/s00703-016-0462-0>

769 Otieno VO, Anyah RO (2013) CMIP5 simulated climate conditions of the Greater Horn of Africa
770 (GHA). Part I: Contemporary climate. *Climate Dyn* 41: 2081–2097.
771 <https://doi.org/10.1007/s00382-012-1549-z>

772 Pabortsava K, Lampitt RS, and co-authors (2017) Carbon sequestration in the deep Atlantic
773 enhanced by Saharan dust. *Nature Geoscience* 10: 189-194.
774 <https://doi.org/10.1038/NGEO2899>

775 Pan BW, Wang YA, and co-authors (2018) Impacts of Saharan dust on Atlantic regional climate
776 and implications for tropical cyclones. *J Climate* 31: 7621-7644.
777 <https://doi.org/10.1175/JCLI-D-16-0776.1>

778 Panthou G, Lebel T, Vischel T, Quantin G, Sane Y, Ba A, Ndiaye O, Diongue-Niang A, Diopkane
779 M (2018) Rainfall intensification in tropical semi-arid regions: the Sahelian case. *Environ
780 Res Lett* 13: 064013. <https://doi.org/10.1088/1748-9326/aac334>

781 Parker DJ, Burton RR, Diongue-Niang A, Ellis RJ, Felton M, Taylor CM, Thorncroft CD,
782 Bessemoulin P, Tompkins AM (2005) The diurnal cycle of the West African monsoon
783 circulation. *Q J R Meteorol Soc* 131(611):2839–2860. <https://doi.org/10.1256/qj.04.52>

784 Patricola CM, Cook KH (2007) Dynamics of the West African Monsoon under mid-Holocene
785 precessional forcing: Regional climate model simulations. *J Climate* 20: 694–716.
786 <https://doi.org/10.1175/JCLI4013.1>

787 Patricola CM, Cook KH (2008) Atmosphere/vegetation feedbacks: A mechanism for abrupt
788 climate change over Northern Africa. *J Geophys Res Atmos* 113: D18102.
789 <https://doi.org/10.1029/2007JD009608>

790 Peyrille P, Lafore J-P, Boone A (2016) The annual cycle of the West African monsoon in a two-
791 dimensional model: Mechanisms of the rain-band migration. *Q J Roy Meteorol Soc* 142:
792 1473–1489. <https://doi.org/10.1002/qj.2750>

793 Pokam WM, Bain CL, Chadwick RS, Graham R, Sonwa DJ, Kamga FM (2014) Identification of
794 processes driving low-level westerlies in West Equatorial Africa. *J Climate* 27: 4245–4262.
795 <https://doi.org/10.1175/JCLI-D-13-00490.1>

796 Pokam WM, Djiotang LAT, Mkankam FK (2012) Atmospheric water vapor transport and
797 recycling in equatorial central Africa through NCEP/NCAR reanalysis data. *Clim Dyn* 38:
798 1715–1729. <https://doi.org/10.1007/s00382-011-1242-7>

799 Polo I, Rodríguez-Fonseca B, Losada T, García-Serrano J (2008) Tropical Atlantic variability
800 modes (1979–2002). Part I: Time-evolving SST modes related to West African rainfall. *J*
801 *Climate* 21: 6457–6475. <https://doi.org/10.1175/2008JCLI2607.1>

802 Pu B, Cook KH (2010) Dynamics of the West African westerly jet. *J Clim* 23: 6263–6276.
803 <https://doi.org/10.1175/2010JCLI3648.1>

804 Pu B, Cook KH (2012) Role of the West African westerly jet in Sahel rainfall variations. *J Clim*
805 25: 2880-2896. <https://doi.org/10.1175/JCLI-D-11-00394.1>

806 Rennick MA (1976) The generation of African waves. *J Atmos Sci* 33: 1955-1969.
807 [https://doi.org/10.1175/1520-0469\(1976\)033<1955:TGOAW>2.0.CO;2](https://doi.org/10.1175/1520-0469(1976)033<1955:TGOAW>2.0.CO;2)

808 Riddle EE, Cook KH (2008) Abrupt rainfall transitions over the Greater Horn of Africa:
809 Observations and regional model simulations. *J Geophys Res Atmos* 113: D15109.
810 <https://doi.org/10.1029/2007JD009202>

811 Roberts AJ, Woodage MJ, Marsham JH, Highwood EJ, Ryder CL, McGinty W, Wilson S, Crook
812 J (2018) Can explicit convection improve modelled dust in summertime West Africa?
813 *Atmos Chem Phys* 18: 9025-9048. <https://doi.org/10.5194/acp-18-9025-2018>

814 Rodríguez-Fonseca B, Mohino E, Mechoso CR, Caminade C, and co-authors (2015) Variability
815 and predictability of West African droughts: A review on the role of sea surface
816 temperature anomalies. *J Climate* 28: 4034-4060. <https://doi.org/10.1175/JCLI-D-14-00130.1>

818 Rowell DP (2003) The impact of Mediterranean SSTs on the Sahelian rainfall season. *J Climate*
819 16: 849–862. [https://doi.org/10.1175/1520-0442\(2003\)016,0849:TIOMSO.2.0.CO;2](https://doi.org/10.1175/1520-0442(2003)016,0849:TIOMSO.2.0.CO;2)

820 Rowell DP, Booth BBB, Nicholson SE, Good P (2015) Reconciling past and future rainfall trends
821 over East Africa. *J Climate* 28: 9768-9788. <https://doi.org/10.1175/JCLI-D-15-0140.1>

822 Rowell DP, Chadwick R (2018) Causes of the uncertainty in projections of tropical terrestrial
823 rainfall change: East Africa. *J. Climate* 31: 5977-5995.

824 Sanogo S, Fink AH, Omotosho JA, Ba A, Redl R, Ermert V (2015) Spatio-temporal characteristics
825 of the recent rainfall recovery in West Africa. *Int J Climatol* 35(15): 4589–4605.
826 <https://doi.org/10.1002/joc.4309>

827 Schlueter A, Fink AH, Knippertz P, Vogel P (2019) A systematic comparison of tropical waves
828 over Northern Africa. Part I: Influence on rainfall. *J Climate* 32: 1501-1523.
829 <https://doi.org/10.1175/JCLI-D-18-0173.1>

830 Schmocker J, Liniger HP, Ngeru JN, Brugnara Y, Auchmann R, Brönnimann (2016) Trends in
831 mean and extreme precipitation in the Mount Kenya region from observations and
832 reanalyses. *Int J Climatol* 36: 1500-1514. <https://doi.org/10.1002/joc.4438>

833 Schwendike JP, Govekar P, Reeder MJ, Wardle R, Berry GJ, Jakob C (2014) Local partitioning
834 of the overturning circulation in the tropics and the connection to the Hadley and Walker
835 circulations. *J Geophys Res Atmos* 119: 1322-1339.
836 <https://doi.org/10.1002/2013JD020742>

837 Seth A, Rauscher SA, Biasutti M, Giannini A, Camargo SJ, Rojas M (2013) CMIP5 projected
838 changes in the annual cycle of precipitation in monsoon regions. *J Clim* 26: 7328–7351.
839 <https://doi.org/10.1175/JCLI-D-12-00726.1>

840 Simmons AJ (1977) Note on instability of African easterly jet. *J Atmos Sci* 34: 1670-1674.
841 [https://doi.org/10.1175/1520-0469\(1977\)034<1670:ANOTIO>2.0.CO;2](https://doi.org/10.1175/1520-0469(1977)034<1670:ANOTIO>2.0.CO;2)

842 Spracklen DV, Baker JCA, Garcia-Carreras L, Marsham JH (2018) The effects of tropical
843 vegetation on rainfall. *Annu Rev Environ Resour* 43: 193-218.
844 <https://doi.org/10.1146/annurev-environ-102017-030136>

845 Suárez-Moreno R, Rodríguez-Fonseca B, Barroso JA, Fink AH (2018) Interdecadal changes in the
846 leading ocean forcing of Sahelian rainfall interannual variability: Atmospheric dynamics
847 and role of multidecadal SST background. *J Climate* 31: 6687-6710.
848 <https://doi.org/10.1175/JCLI-D-17-0367.1>

849 Sultan B, Janicot J (2000), Abrupt shift of the ITCZ over West Africa and intra-seasonal
850 variability, *Geophy Res Lett* 27: 3353–3356. <https://doi.org/10.1029/1999GL011285>

851 Sultan B, Janicot S (2003), The West African monsoon dynamics Part II: The preonset and onset
852 of the summer monsoon, *J. Clim* 16: 3407-3427. [https://doi.org/10.1175/1520-0442\(2003\)016<3407:TWAMDP>2.0;2](https://doi.org/10.1175/1520-0442(2003)016<3407:TWAMDP>2.0;2)

853 Taylor CM, Belušić D, Guichard F, Parker DJ, Vischel T, Bock O, Harris PP, Janicot S, Klein C,
854 Panthou G (2017), Frequency of extreme Sahelian storms tripled since 1982 in satellite
855 observations, *Nature* 544: 475-478. <https://doi.org/10.1038/nature22069>

856 Taylor CM, Lambin EF, Stephenne N, Harding RJ, Essery RLH (2002) The influence of land use
857 change on climate in the Sahel. *J Climate* 15: 3615–3629. [https://doi.org/10.1175/1520-0442\(2002\)015,3615:TIOLUC.2.0.CO;2](https://doi.org/10.1175/1520-0442(2002)015,3615:TIOLUC.2.0.CO;2)

859 Taylor CM, Fink AH, Klein C, Parker DJ, Guichard F, Harris PP, Knapp KR (2018) Earlier
860 seasonal onset of intense mesoscale convective systems in the Congo Basin since 1999.
861 *Geophys Res Lett* 45: 13458-13467. <https://doi.org/10.1029/2018GL080516>

862 Taylor KE, Stouffer RJ, Meehl GA (2012) An overview of CMIP5 and the experiment design.
863 *Bull Am Meteorol Soc* 93: 485–498. <https://doi.org/10.1175/BAMS-D-11-00094.1>

864 Thorncroft CD (1995) An idealized study of African easterly waves. III: More realistic basic states.
865 *Q J R Meteorol Soc* 121: 1589–1614. <https://doi.org/10.1002/qj.49712152706>

866 Thorncroft CD, Blackburn M (1999) Maintenance of the African Easterly jet. *Q J Roy Meteorol
867 Soc* 125: 763-786. <https://doi.org/10.1002/qj.49712555502>

868 Thorncroft CD, Hall NJM, Kiladis GN (2008) Three-dimensional structure and dynamics of
869 African easterly waves. Part III: Genesis. *J Atmos Sci* 65: 3596-3607.
870 <https://doi.org/10.1175/2008JAS2575.1>

872 Thorncroft CD, Hoskins BJ (1994) An idealized study of African easterly waves. II: A nonlinear
873 view. *Q J R Meteorol Soc* 120: 983-1015. <https://doi.org/10.1002/qj.49712051810>

874 Thorncroft CD, Nguyen H, Zhang C, Peyrillé P (2011) Annual cycle of the West African monsoon:
875 Regional circulations and associated water vapour transport. *Quart J Roy Meteor Soc* 137:
876 129–147. <https://doi.org/10.1002/qj.728>

877 Ummenhofer CC, Kulüke M, Tierney JE (2018) Extremes in East African hydroclimate and links
878 to Indo-Pacific variability on interannual to decadal timescales. *Clim Dyn* 50: 2971-2991.
879 <https://doi.org/10.1007/s00382-017-3786-7>

880 Vizy EK, Cook KH (2002) Development and application of a mesoscale climate model for the
881 tropics: Influence of sea surface temperature anomalies on the West African monsoon. *J
882 Geophys Res Atmos* 107: 4023. <https://doi.org/10.1029/2001JD000686>

883 Vizy EK, Cook KH (2017) Seasonality of the observed amplified Sahara warming trend and
884 implications for Sahel rainfall. *J Climate* 30: 3073-3094. [https://doi.org/10.1175/JCLI-D-16-0687.1](https://doi.org/10.1175/JCLI-D-
885 16-0687.1)

886 Vizy EK, Cook KH (2018a) Mesoscale convective systems and nocturnal rainfall over the West
887 African Sahel: Role of the Inter-tropical front. *Clim Dyn* 50: 587-614.
888 <https://doi.org/10.1007/s00382-017-3628-7>

889 Vizy EK, Cook KH (2018b) Understanding the summertime diurnal cycle of precipitation over
890 sub-Saharan West Africa: Regions with daytime rainfall peaks in the absence of significant
891 topographic features. *Clim. Dyn.* <https://doi.org/10.1007/s00382-018-4315-z>

892 Vizy EK, Cook KH, Crétat J, Neupane N (2013) Projections of a wetter Sahel in the 21st century
893 from global and regional models. *J Climate* 26: 4664-4687. [https://doi.org/10.1175/JCLI-D-12-00533.1](https://doi.org/10.1175/JCLI-
894 D-12-00533.1)

895 Wang G, Yu M, Xue Y (2016) Modeling the potential contribution of land cover changes to the
896 late twentieth century Sahel drought using a regional climate model: Impact of lateral
897 boundary conditions. *Clim Dyn* 47: 3457-3477. <https://doi.org/10.1007/s00382-015-2812-x>

898

899 Ward MN (1998) Diagnosis and short-lead time prediction of summer rainfall in tropical North
900 Africa at interannual and multidecadal timescales. *J Climate* 11: 3167–3191.
901 [https://doi.org/10.1175/1520-0442\(1998\)011,3167:DASLTP.2.0.CO;2](https://doi.org/10.1175/1520-0442(1998)011,3167:DASLTP.2.0.CO;2)

902 Washington R, James R, Pearce H, Pokam WM, Moufouma-Okia W (2013) Congo rainfall
903 climatology: can we believe the climate models? *Phil Trans R Soc. B* 368: 20120296.
904 <https://doi.org/10.1098/rstb.2012.0296>

905 Weller E, Cai W (2013) Realism of the Indian Ocean dipole in CMIP5 models: The implications
906 for climate projections. *J Climate* 26: 6649-6659. <https://doi.org/10.1175/JCLI-D-12-00807.1>

907

908 Williams AP, Funk C (2011) A westward extension of the warm pool leads to a westward
909 extension of the Walker circulation, drying eastern Africa. *Climate Dyn* 37: 2417–2435.
910 <https://doi.org/10.1007/s00382-010-0984-y>

911 Wu M-L C, Reale O, Schubert WD, Suarez MJ, Koster RD, Pegion PJ (2009) African Easterly
912 Jet: Structure and maintenance. *J Clim* 22: 4459-4480.
913 <https://doi.org/10.1175/2009JCLI2584.1>

914 Yang W, Seager R, Cane MA, Lyon B (2014) The East African long rains in observations and
915 models. *J Climate* 27: 7185-7202. <https://doi.org/10.1175/JCLI-D-13-00447.1>

916 Yang W, Seager R, Cane MA, Lyon B (2015) The annual cycle of the East African precipitation.
917 *J Climate* 28:2385–2404. <https://doi.org/10.1175/JCLI-D-14-00484.1>

918 Yang W, Seager R, Cane MA, Lyon B (2015b) The Rainfall Annual Cycle Bias over East Africa
919 Induced by CMIP5 Coupled Climate Models. *J Climate* 28: 9789-9802.
920 <https://doi.org/10.1175/JCLI-D-15-0323.1>

921 Zhang G, Cook KH (2014) West African monsoon demise: Climatology, interannual variations,
922 and relationship to seasonal rainfall. *J Geophys Res Atmos* 119: 10175–10193.
923 <https://doi.org/10.1002/2014JD022043>

924 Zhang G, Cook KH, Vizy EK (2016a) The diurnal cycle of warm season rainfall over West Africa.
925 Part I: Observational analysis. *J Climate* 29: 8423-8437. <https://doi.org/10.1175/JCLI-d-15-0874.1>

927 Zhang G, Cook KH, Vizy EK (2016b) The diurnal cycle of warm season rainfall over West Africa.
928 Part II: Convection-permitting simulations. *J Climate* 29: 8439-8454. <https://doi:10.1175/JCLI-d-15-0875.1>

930 Zhou LM, Tian YH, Myneni RB, Ciais P, Saatchi S, Liu YY, Piao SL, Chan HS, Vermote EF, and
931 co-authors (2014) Widespread decline of Congo rainforest greenness in the past decade.
932 *Nature* 509: 86-89. <https://doi.org/10.1038/nature13265>

933 Zwiers FW, von Storch H (1995) Taking serial correlation into account in tests of the mean. *J Clim*
934 8: 336-351. [https://doi.org/10.1175/1520-0442\(1995\)008<0336:TSCIAI>2.0.CO;2](https://doi.org/10.1175/1520-0442(1995)008<0336:TSCIAI>2.0.CO;2)

935

936

937

Table 1. Linear slopes of Congo Basin (10°E-30°E, 5°S-5°N) precipitation with confidence levels that account for autocorrelation using the method of Zwiers and von Storch (1995). Asterisks indicate significant drying at the 90th (*), 95th (**), and 99th (***) percentiles.

Dataset	Annual		DJF		MAM		JJA		SON	
	1979-2017	1998-2017	1979-2017	1998-2017	1979-2017	1998-2017	1979-2017	1998-2017	1979-2017	1998-2017
TRMM	----	-0.114	----	-0.093	----	0.024	----	-0.467**	----	-0.001
GPCP	-0.015	-0.035	0.093	0.058	-0.083	0.116	-0.099	-0.420**	0.055	0.064
CHIRPS	-0.061**	-0.089	-0.059	-0.246	-0.027	0.293*	-0.04	-0.280*	-0.113	-0.157
ARC2	-0.147	0.065	-0.139	-0.065	-0.137	0.576***	-0.11	-0.162	-0.244*	-0.052
CMORPH	----	-0.516***	----	-0.879***	----	-0.07	----	-0.723***	----	-0.531**
PERSIANN	-0.027	-0.065	0.053	-0.041	-0.118	0.11	-0.113	-0.379**	0.043	-0.003

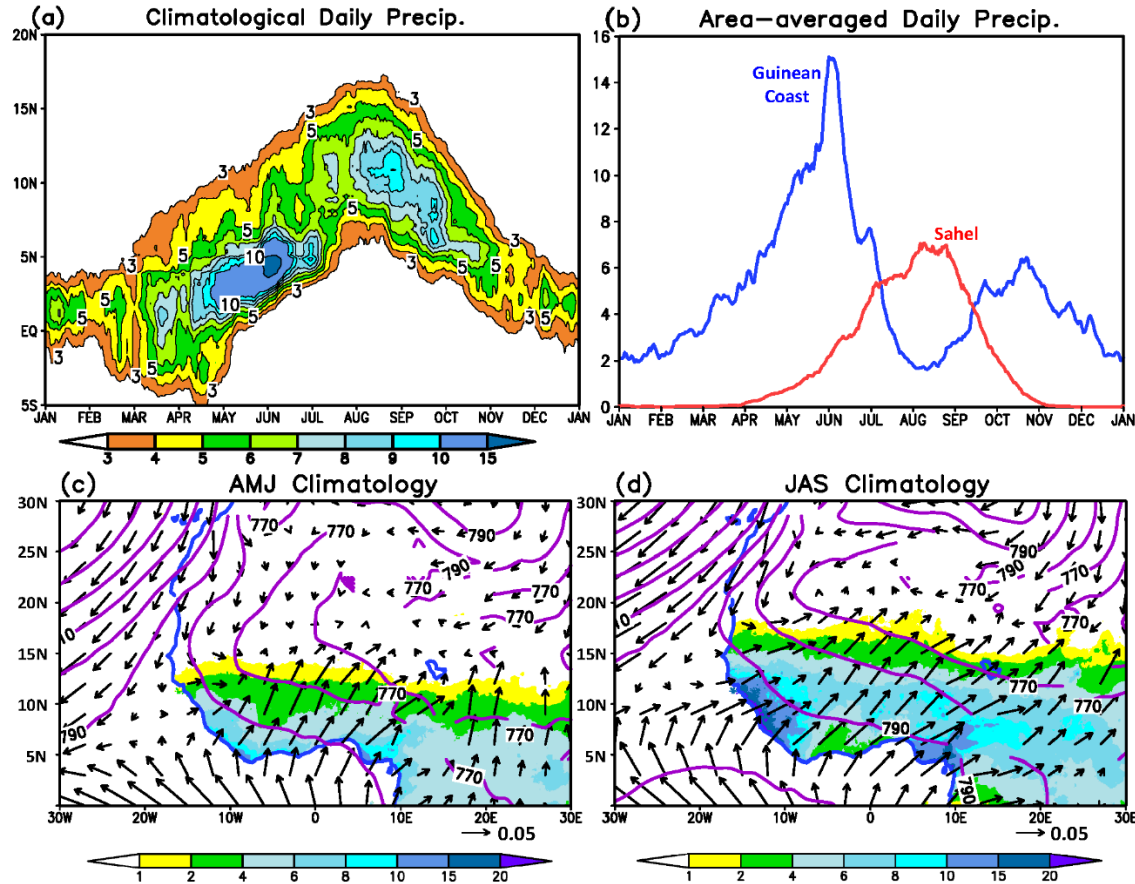


Figure 1. (a) 1998-2017 climatological daily TRMM TMPA precipitation (mm day^{-1}) averaged over West Africa between 12°W - 6°E and smoothed using an 11-day running mean filter. (b) 1998-2017 climatological smoothed daily TRMM TMPA precipitation averaged over the Guinean Coast (3°N - 6°N ; 12°W - 6°E) and Sahel (12°N - 15°N ; 12°W - 6°E) regions. 1981-2018 climatological (c) April – June (AMJ), and (d) July – September (JAS) CHIRPS precipitation (shaded; mm day^{-1}) and ERAI reanalysis 925 hPa geopotential heights (contours; m) and moisture transport vectors ($\text{kg m kg}^{-1} \text{ s}^{-1}$).

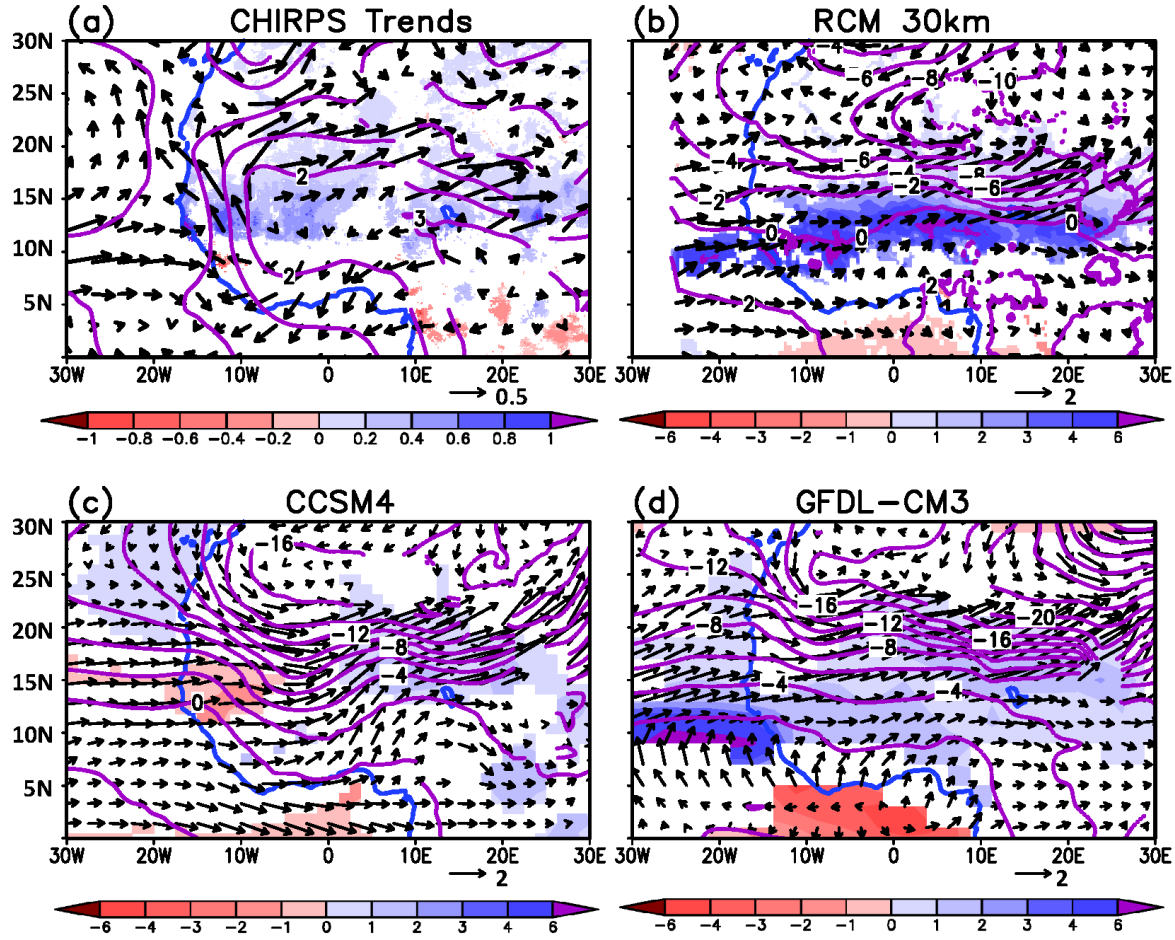


Figure 2. (a) CHIRPS V2.0 1981-2018 July – September precipitation trends (shaded; mm day^{-1} per decade) with 925-hPa geopotential height (m per decade), and wind (m s^{-1} per decade) trends from the ERAI reanalysis. Only precipitation trends statistically significant at the 90% level of confidence according to a Student's *t*-test are shaded. Late 21st century (2081-2100) July – September precipitation (shaded; mm day^{-1}), 925 hPa scaled geopotential height (contours; m) and winds (vectors; m s^{-1}) anomalies projections for the (b) Vizy et al. (2013) 30-km RCM simulation, and the CMIP5 RCP8.5 (c) CCSM4, and (d) GFDL CM3. Only precipitation trends and anomalies statistically significant at the 95% level of confidence according to a Student's *t* test are shaded.

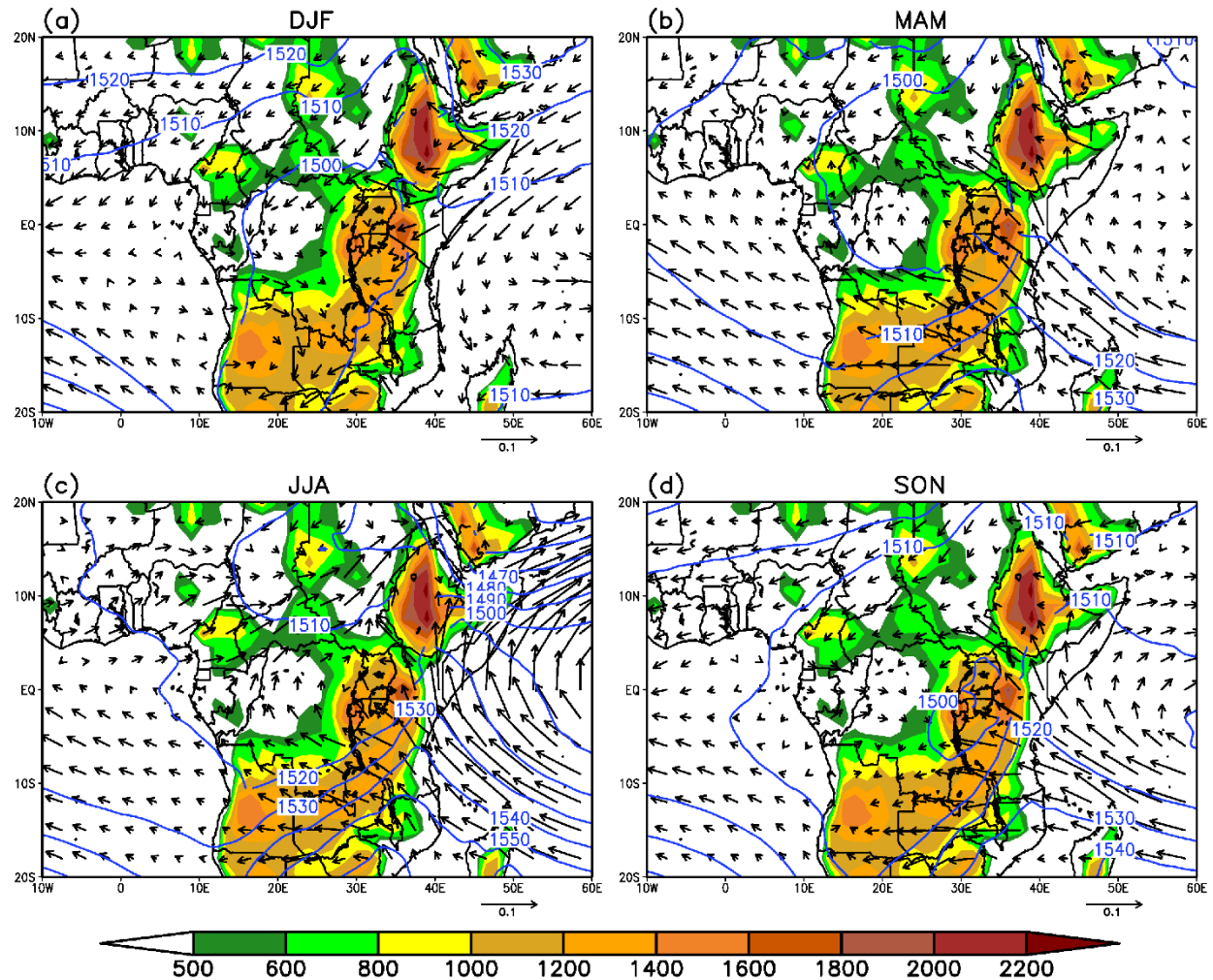


Figure 3. ERAI 1981-2018 climatological 850 hPa moisture flux transport (vectors; $\text{kg m kg}^{-1} \text{ s}^{-1}$) and geopotential height (contours; m) for (a) December – February (DJF) (b) March – May (MAM), (c) June – August (JJA), and (d) September – November (SON). Shading denotes the topography (m) as resolved in the ERAI at 1.5° resolution.

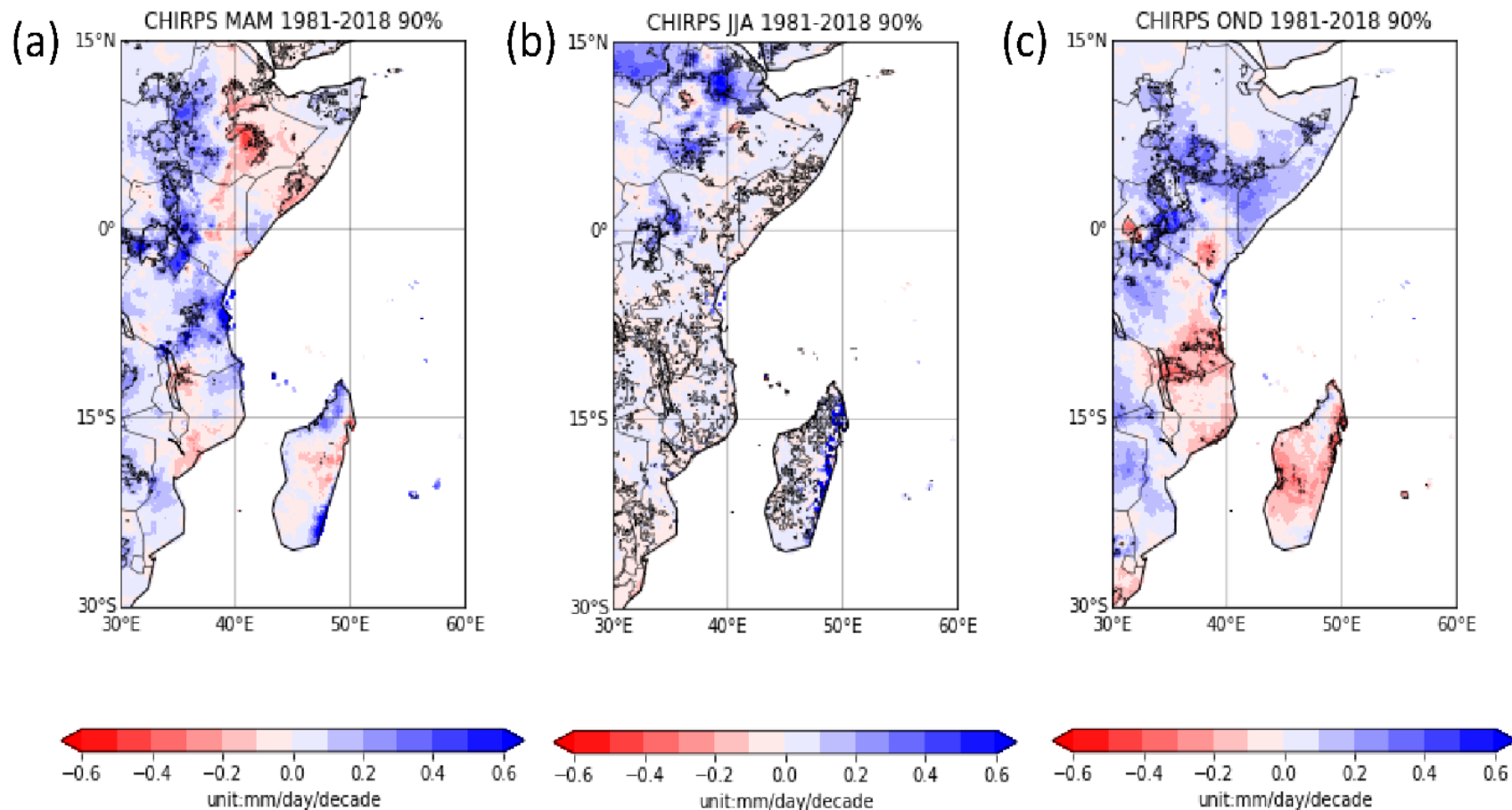


Figure 4. CHIRPS V2.0 1981-2018 precipitation trends (shaded; mm day-1 per decade) for (a) March-May (MAM), (b) June – August (JJA), and (c) October – December (OND). Only precipitation trends and anomalies statistically significant at the 95% level of confidence according to a Student's t test are shaded. (Figure courtesy Siyu Zhao.)

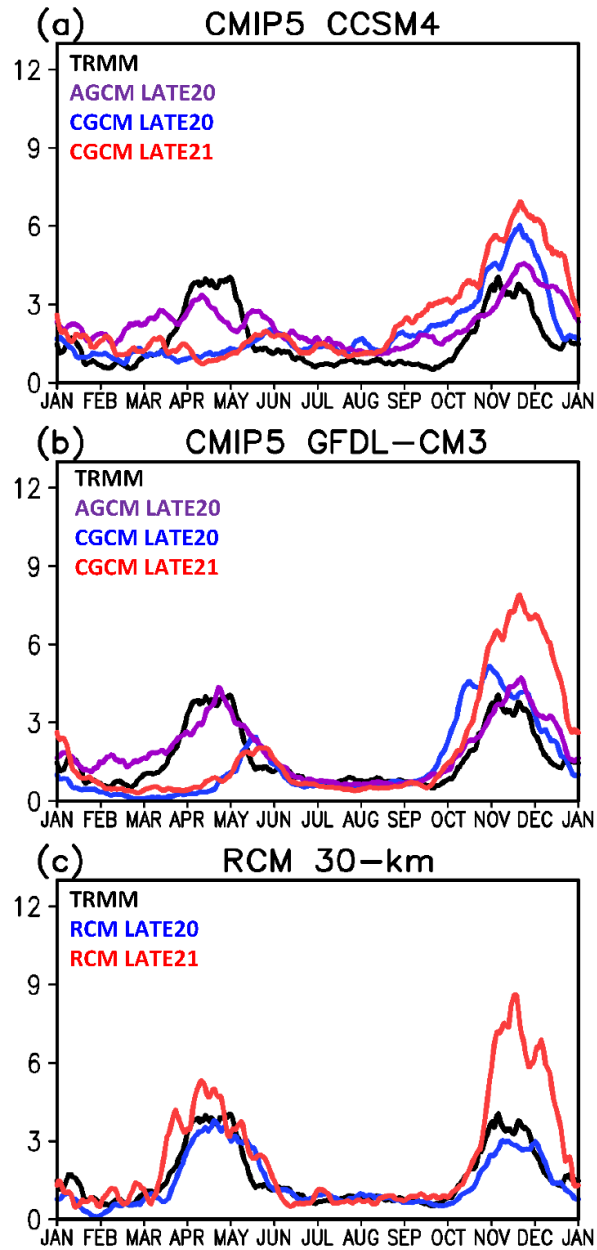


Figure 5. (a) Daily climatological precipitation (mm day^{-1}) averaged over 35°E - 42°E and 3°S - 3°N and 1986-2005 from atmosphere-only (AGCM LATE20; purple) and coupled (CGCM LATE20; blue) versions of the CCSM4 GCM. The black line denotes climatological TRMM TMPA precipitation observations, and the red line is precipitation from CGCM simulations for 2081-2100 (CGCM LATE21) with greenhouse gas increases from the RCP8.5 emissions scenario. (b) Same as (a) but using output from GFDL-CM3 GCM simulations. (c) Same as (a) but using output from atmosphere-only regional model simulations with 30-km horizontal resolution (Vizy et al. 2013).

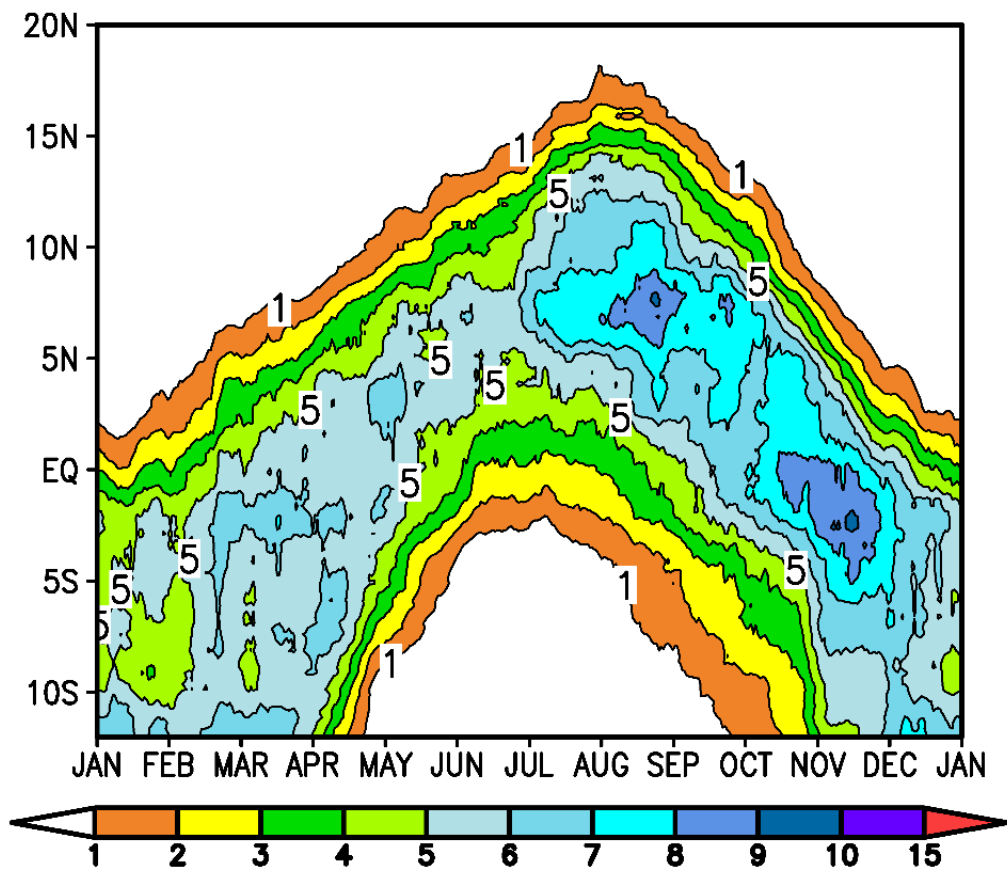


Figure 6. 1998-2018 climatological daily TRMM TMPA precipitation (mm day^{-1}) averaged over the Congo Basin/central Africa between 10°E - 30°E and smoothed using an 11-day running mean.